Indian Journal of Engineering & Materials Sciences
Vol. 32, February 2025, pp. 56-69
DOI: 10.56042/ijems.v32i01.11672

Synthesis, characterization and selection of optimal constituents of magnetorheological fluid for damper application

Subash Acharya[a,b], N P Puneet[c], Rangaraj M Desai[d], Vishal Sundaram[a] & Hemantha Kumar[a]*

[a]Department of Mechanical Engineering, National Institute of Technology Karnataka, Surathkal, Mangalore NIT 575 025, India

[b]Department of Mechanical & Industrial Engineering, Manipal Institute of Technology, Manipal Academy of Higher Education, Manipal, Karnataka 576 104, India

[c]Department of Automobile Engineering, Dayananda Sagar College of Engineering, Shavige Malleswara Hill, Kumaraswamy Layout, Bangalore 560 111.

[d]Department of Mechanical Engineering, Graphic Era Deemed to be University, Dehradun, Uttarakhand 248 002, India

Received:12 July 2024 ; accepted: 11 January 2025

Magnetorheological (MR) dampers are a category of energy dissipating devices that employ magnetorheological fluids which undergoes drastic change in its behaviour under the presence of magnetic stimulus. The damping characteristics of an MR damper predominantly depends on the dimensions of damper and on the constituents of MR fluid (MRF). In this work, an optimal MRF composition suitable for a monotube MR damper has been selected from six prepared MRF based on optimization. Initially, MR damper piston dimensions have been obtained by means of optimization. The damper has been fabricated and filled with commercial MRF 132DG^{TM} fluid (Lord Corporation) and its performance has been tested. The experimental results have been validated with computational results. In the next part of the study, MRF samples composed of three particle weight fractions of fine and coarse sized iron particles have been synthesized and the rheological properties have been measured and compared with those of commercial MR fluid. The force-displacement characteristics of damper employing synthesized MRF have been determined with and without application of current to damper coil. Finally, by means of Multi-Objective Genetic Algorithm, optimum iron particle size and weight fraction have been selected from the pareto front solutions.

Keywords: Damping coefficient, Genetic algorithm, Magnetorheological fluid, MR damper, Optimization

1 Introduction

Magnetorheological fluids belong to adaptive and field responsive fluids[1,2] which was discovered and reported by Jacob Rabinow in the year 1948[3]. They are composed of magnetic powder of micron size in a carrier fluid. The randomly dispersed particles in the MRF acquire a dipole moment when magnetic field is applied and align along the same resulting in a chainlike shape. Hence, its rheological properties namely viscosity and shear stress can be varied in real time instantaneously and reversibly. This controllable property has been made use of in a number of applications such as robotics, engine mounts, shock absorbers, clutches, seat dampers, polishing devices, brakes, valves, vibration control dampers, prosthetic knee and several prospective applications[4-11]. Although there are lot of research works performed on MR devices, very few have realized successful implementation[12]. MR dampers have attracted significant interest from the research community because of their customizable damping capability, lesser current demands, rapid response, simple and ease of control in comparison with standard passive dampers. The damping force is the crucial factor and would be effectively enhanced by strategically configuring the piston of the damper. Many researchers have computed optimal dimensions of MR damper by means of finite element analysis[13-16]. Nguyen *et al.*[17] proposed an analytical approach to obtain the optimal size of a single-coil as well as two-coil type annular piston of MR damper. The goal was to maximize the damper force. Parlak *et al.*[18] conducted an experiment using the Taguchi design approach to create and evaluate nine variations of MR dampers. The goal was to identify the most effective configuration of MR dampers that would maximize both the damping ratio as well as the damping force. Xu *et al.*[19] performed magnetic design of a shear-valve mode MR damper for the purpose of mitigating earthquakes. The optimal dimensions for the MR

*Corresponding author (E-mail: hemantha@nitk.edu.in)

damper were determined using a constrained optimization function using MATLAB™ software for achieving a damping force of 200 kN for a piston speed of 100 mm/s, while ensuring a dynamic range higher than 15. The size and design of a twin-tube MR damper for car suspension was determined by Desai *et al.*[20,21]. The damper underwent testing at different frequencies and currents, and the test data was verified against analytical results. Puneet *et al.*[22] designed a MR damper for a vehicle and modelled the hysteretic behaviour of MR damper by using Kwok model. The quarter car simulation using mathematical model and the experimental quarter car testing exhibited vibration suppression capability of MR damper.

The MR damper performance can also be enhanced using MR fluid of appropriate composition. By means of particle swarm optimization techniques based on single and multi-objectives, Gurubasavaraju *et al.*[23] obtained optimum percentage of iron powder in MRF for damper that resulted in very high shear stress and damping force. Mangal and Sharma[24] examined parameters, including carrier fluid, size of iron particle, additives' concentrations and percentage of iron particles, in order to determine the optimal ingredients for magnetorheological fluids (MRFs). The goal was to maximize the field-induced viscosity and yield stress. Acharya *et al.*[25] determined optimum particle mass fraction, its diameter, and carrier oil viscosity of MRF for a single disk MR brake using Multi-Objective Genetic Algorithm (MOGA) optimization with the intension for maximizing the on-state braking torque and minimizing the off-state torque. Acharya *et al.*[26] used MOGA optimization to find optimal particle size and mass fraction for MR beam with the objectives of minimizing mass of MR fluid and maximizing damping ratio. In another work, Acharya *et al.*[27] used MOGA optimization technique to select optimal percentage of iron particle and particle diameter for use in MR damper. Maximizing damping force and minimizing of zero-field viscosity were considered as objectives of optimization. The damping forces were calculated using magnetostatic analyses of MR damper to compute magnetic field intensity in MRF gap, followed by calculation of yield stress for different MRF. The yield stress values for different MRF were substituted in the governing force equation of the MR damper. However, damping force was not measured experimentally.

This work provides an optimum MRF for an MR damper based on optimizing the damper performance as determined experimentally using various produced MRF. A shear mode magnetorheological damper with a monotube design was initially constructed to meet specific requirements for dynamic range and damping force using a constrained optimization function. A damper was constructed with optimal dimensions and then filled with MRF 132DG™ fluid to determine the damping behaviour of the damper using a damper testing machine. Magnetic field intensities in the MR fluid gap at 1 A and 2 A currents were calculated using magnetostatic analyses in the ANSYS™ workbench software in order to verify the findings. By taking MRF yield stress as the base, which is influenced by the distribution of magnetic fields in the shear flow gap, the damper force was estimated. The force values that were computed and those that were obtained experimentally were compared. Additionally, MRFs with particle sizes of 2.9 and 8.27 microns were prepared with each consisting of 60%, 70%, and 80% weight fractions of ferromagnetic particles. Using a rheometer, the flow curves of the prepared MRF and MRF 132DG™ were measured, and the MRF's sedimentation stability was obtained. The damper characteristics of an MR damper with magneto-rheological fluid that was made in-house were assessed at various frequencies, with and without current inputs, and for piston's sinusoidal displacement of ±10 mm. The energy dissipated was calculated using the area encompassed by the characteristic force v/s displacement curves, and the corresponding damping coefficient was subsequently determined using this information. Lastly, by means of MOGA optimization, the optimum weight fraction and particle size of iron powder were found based on maximizing the on-state damping coefficient (when a magnetic field is present) and minimizing the off-state damping coefficient (when a magnetic field is absent).

2 Materials and Methods

2.1 MR damper design

A monotube damper is commonly utilized in MR devices because of its ease of use, small size, and capacity to operate well in any installed orientation. As seen in Figure 1, it comprises of a single reservoir that is filled with MRF and has a piston that reciprocates within it. A copper coil is wrapped around the piston's core and the lead wires are used for external power source connection which are available from the end of piston rod. An appropriate seal is incorporated into the damper housing's rod end to prevent MRF leaking when the piston rod reciprocates.

Viscosity-induced (off-state) and field-dependent (on-state) shear stresses are used to represent the MRF's overall shear stress when a magnetic field is supplied. Hence, the overall damping force (F) for a shear mode magnetorheological damper is the total of the friction force (F_f), field-induced (on-state) damping force (F_τ), and viscous (off-state) damping force (F_μ).

$$F = F_\tau + F_\mu + F_f \quad \ldots (1)$$

Neglecting the friction force, the damping force is expressed based on parallel plate Bingham model by equation (2)[28-29].

$$F = \left(2.07 + \frac{12Q\mu}{12Q\mu + 0.4wg^2\tau_y}\right)\frac{\tau_y L A_p}{g}\,\mathrm{sgn}(v) + \left(1 + \frac{wgv}{2Q}\right)\frac{12\mu Q L_p A_p}{wg^3} \quad \ldots (2)$$

where,

$$A_p = \frac{\pi\left(D_p^2 - d_r^2\right)}{4} \quad \ldots (3)$$

$$w = \pi\left(\frac{g}{2} + D_p + \frac{g}{2}\right) \quad \ldots (4)$$

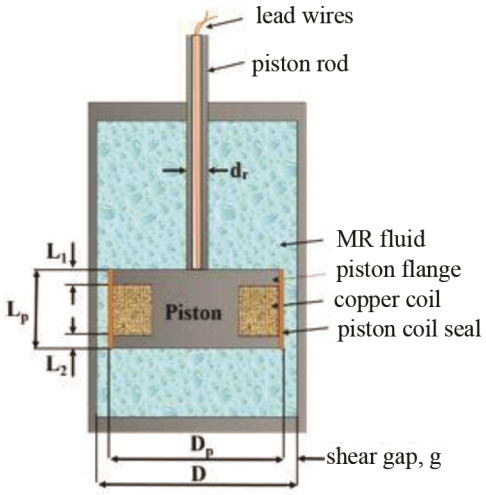

Fig. 1 — Representative drawing of a shear mode MR damper.

$$Q = vA_p \quad \ldots (5)$$

where, Q: volumetric flow rate (m^3/s), v:velocity of the piston (m/s), μ: viscosity of MRF in the absence of magnetic field (Pa-s), w: average circumference of MRF shear gap (m), g: MRFshear gap (m), τ_y: shear yield stress (Pa),L $(= L_1 + L_2)$ (m) : height of piston flange (m), A_p: cross-sectional area of piston (m^2), L_p: piston height (m), D_p: piston diameter (m), d_r: piston rod diameter (m).

The ratio of the overall damping force to the uncontrollable forces is called as dynamic range (K_{dy}) and is expressed by equation (6). The viscous damping force is the uncontrollable force[18].

$$K_{dy} = \frac{F_\mu + F_\tau}{F_\mu} \quad \ldots (6)$$

The properties of MRF 132DG™ were considered for the design of the damper. This fluid has a viscosity[30] of 0.114 Pa-s specified at shear rates in the range between 800 /s and 1200 /s (40°C) and Figure 2(a) shows its magnetization (B-H) curve. Figure 2(b) displays the B-H curve for the SAE 1020 steel[31]. The relationship between yield stress (τ_y in kPa) of the MRF 132DG™ and magnetic field (H in kA/m) is expressed by equation (7)[32]. It is obtained by measuring the flow curves at different magnetic fields, determining its yield stress at different magnetic fields and curve fitting these values.Equation (7) gives the yield stress of MRF 132DG™ at a magnetic field of 75 kA/m, which is 22.74 kPa.

$$\tau_y = -0.8239 + 0.3668 \times H - 7 \times 10^{-4} \times H^2 \quad \ldots (7)$$

The optimal MRF shear gap for MR devices falls between 0.25 to 2 mm[33]. A MRF shear gap of 0.5 mm was used, as a smaller gap leads to a greater magnetic field strength and therefore a greater damping force.

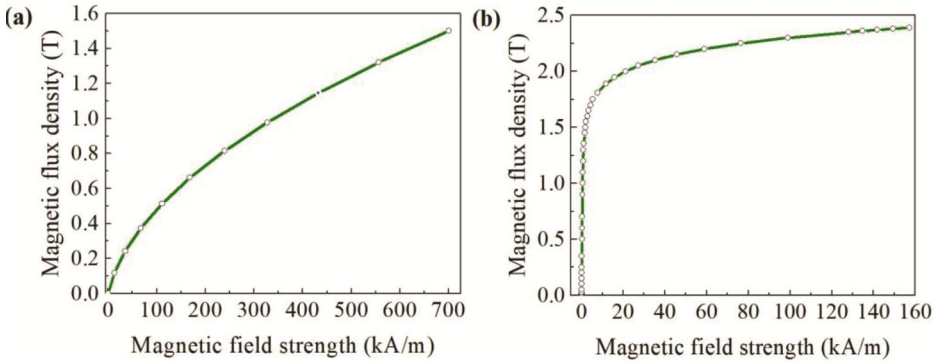

Fig. 2 — Magnetization curve of (a) MRF 132DG™ and (b) SAE 1020 steel.

Nevertheless, a separation smaller than 0.5 mm leads to a decrease in dynamic range due to a significant rise in viscous force relative to the increase in on-state damping force[34]. The design parameters consist of the diameter of the piston, the diameter of the piston rod, the height of the piston, and the height of its flange. The goal was to achieve a damper force of 1000 N with a piston velocity of 0.2 m/s and a dynamic range greater than 4. The damper piston was designed using the MATLAB™ software[19], with a *fmincon* constrained non-linear optimization function.

2.2 Performance of the MR damper

The performance of the MR damper with standard MRF 132DG™ fluid was experimentally determined using a damper testing equipment (Make: HEICO) shown in Figure 3. A hydraulic powerpack delivers the necessary power to the hydraulic actuator, which can generate an excitation force of 20 kN and has a end-to-end stroke length of 150 mm at velocities of up to 1.2 m/s. The servo controller (Make: Moog) controls the frequency of excitation. The force sensor is positioned at the lower end of the lower jaw and measures the total damping force. The software interface is used to specify the piston stroke, excitation frequency, and the excitation type. Data obtained from force and position sensors are stored in the software for subsequent analysis. Current to damper coil is supplied by means of DC power source (Make: ScientiFic).

The MRF 132DG™ fluid was injected into the damper, which was thereafter securely positioned between the upper and lower jaws of the damper testing equipment. Initially, the piston was subjected to a movement of ± 10 mm for 10 cycles at a frequency of 0.5 hertz in order to ensure that the magnetorheological fluid (MRF) was evenly distributed within the damper cylinder. Experiments were conducted on the MR damper using a sinusoidal excitation with a piston stroke length of ± 10mm and frequencies of 0.5 hertz, 1.0 hertz, 2.0 hertz, and 4.0 hertz. The tests were performed both without current and with direct current inputs of 1 A and 2 A.

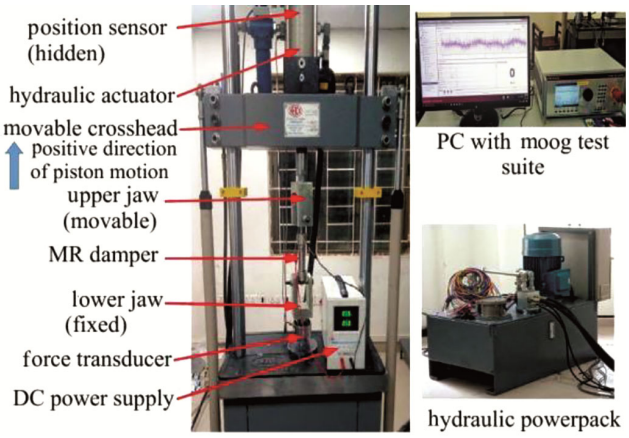

Fig. 3 — Damper testing facility.

2.3 Computational damping force

Computational damping force was obtained using two step method. First, magnetostatic analyses were carried out to determine the MRF gap's magnetic field intensity. Next, based on the magnetostatic analysis results the yield shear stress and consequently damping force were calculated using analytical equations.

The magnetic field intensity in the MRF shear gap near the piston flange regulates the MR damper force. The distribution of magnetic field strength was computed using magnetostatic analyses in ANSYS™ Workbench software. A quarter of the piston was modelled, with properties of material specified to the piston core, cylinder, piston rod, MR fluid in the cylinder, copper coil and the piston coil seal. There are three regions of MRF, one above and one below the piston and third one in the circumferential annular gap between the piston and cylinder i.e. MRF shear gap. About the symmetry plane, the magnetic field lines were described in a parallel manner. The investigations were carried out using a voltage of 12 V and current amplitudes of 1 A and 2 A. The distribution of field strength in the gap of the MRF is extracted for a height of 6 mm from both the top and bottom of piston. The values are used to evaluate the yield strength by utilizing equation (7). Next, using the first term of equation (2), the damping force (F_τ) at 1 A and 2 A current conditions was determined.

2.4 MR fluid synthesis and characterization

2.4.1 Characterization of iron particles

Carbonyl iron powders (CIP) of fine (Sigma Aldrich, C3518) and coarse (Sigma Aldrich, 44890) powders were used in this study. The size distribution and magnetic characteristics of CIP were measured. Particle Size Analyser (Make: Cilas 1064) having a measurement range of 0.04 to 500 microns was used to measure the size distribution of particles. Further, Vibrating sample magnetometer (Make: Lakeshore, 7410) was utilized to determine magnetic hysteresis curves of the iron powders.

2.4.2 Synthesis of MR fluid

An MRF is a suspension consisting of magnetic iron powder in carrier oil with small quantity of

additives. MRF were synthesized with three CIP weight fractions namely 60%, 70% and 80% each for CIP of coarse and fine sizes. Carrier fluid used is Polyalphaolefin oil (PAO, Exxon Mobil) of 32 centistokes viscosity (@ 40°C). A low viscosity oil was used as the base fluid in order to decrease the off-state force, hence increasing the dynamic range of the damper. In addition, using a carrier fluid with reduced viscosity decreases the response time of magnetorheological fluids (MRF) and improves the ability to disperse settled particles[35]. In order to decrease the agglomeration, fumed silica (Sigma Aldrich) was introduced with a weight percentage of 3% in relation to the carrier oil. In addition, aluminum distearate (Sigma Aldrich) was used in the same amount as the fumed silica to improve the suspension redispersibility[36-37]. During the preparation of MRF, desired mass of each of components of MRF were weighed. The additives were mixed in the base fluid for 4 hours using a mechanical stirrer. Next, iron particles were added to the solution and stirred for a duration of twelve hours to achieve a uniform MRF suspension. The MRF, which consists of weight fractions of coarse CIP at 60%, 70%, and 80%, is referred to as MRFL 60, MRFL 70, and MRFL 80, respectively. Similarly, MRFs consisting of 60%, 70%, and 80% weight fractions of fine CIP are referred to as MRFS 60, MRFS 70, and MRFS 80, respectively.

2.4.3 Rheology testing of prepared MRFs

Rheometer (MCR-702, Anton Paar) depicted in Figure 4 was utilized to determine the shear stress variation with shear rate (flow curves) for the prepared and commercial MRF at different currents. The test conditions are specified using a software (Rheocompass) which is interfaced with the Rheometer and also stores the acquired data for further analyses. A magnetorheological device (MRD) cell generates magnetic field on the test samples depending on the magnitude of current specified in the software.

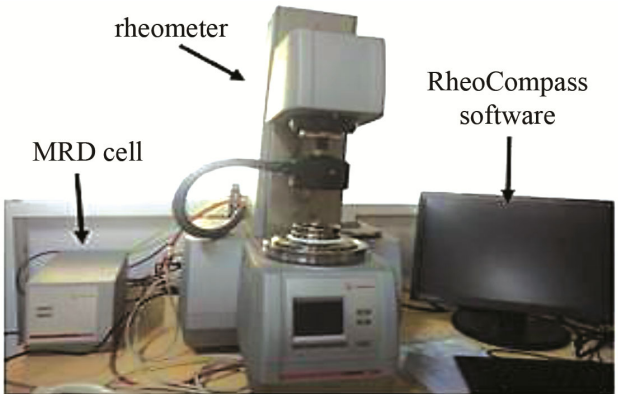

Fig. 4 — Rheometer Setup (Courtesy: Central Research Facility, NITK Surathkal).

The gap between the parallel plates (20 mm diameter) was specified as 0.5 mm and temperature was specified as 25°C during testing. The MRF were mixed properly prior to pouring it on the stationary bottom plate. Prior to testing the MRF[23], the fluids underwent pre-shearing for 20 sec at a shear rate of 10 per sec, followed by a 10-second waiting period to ensure equal distribution of the sample. The samples underwent testing at shear rates that progressively increased from 0.1 /s to 600 /s. The characteristics of the samples were measured at 12 different shear rate values. The experiments were conducted under two conditions: without any electric current (0 A, off-state) and with electric current (on-state) at 1.5 A and 3 A.

2.4.4 Sedimentation stability

The iron particles suspended in the carrier fluid in MRF settle with time due to difference in their densities. The sedimentation ratio is a measure of sedimentation stability of the MRF and were measured for prepared MRF by visually observing the location of boundary between the clear and turbid part of MRF[37]. 10 ml of MRF were poured in graduated cylindrical tubes. After every twelve hours, readings were taken periodically until the particles have completely settled.

2.5 MR damper characteristics employing prepared MRF

The magnetic rheological (MR) damper, filled with various magnetorheological fluids (MRF) manufactured in-house, was subjected to testing at frequencies of 0.5 Hertz, 1 Hertz, 2 Hertz, and 4 Hertz. The damper was tested both without any electrical current and with direct current (DC) inputs of 1 A and 2 A. The testing involved applying a sinusoidal excitation with a piston stroke length of ±10mm.

The enclosed region within the damper's force-displacement plots represents the amount of energy dissipated during a single cycle of upward and downward piston motion. The enclosed region between the force-displacement curves was determined for a frequency of 4 Hertz under both off-state (0A) and on-state (2A) conditions. In addition, the equivalent damping coefficient (C_{eq}) of the damper was determined using equation (8). This value

was calculated by considering the dissipated energy in every cycle (E), the magnitude of excitation (X), and the frequency of excitation (f)[38].

$$C_{eq} = \frac{\mathrm{E}}{2.\pi^2.f.X^2} \quad \ldots(8)$$

2.6 Selection of optimum weight fraction and particle size

To achieve a greater dynamic range of damping, it is crucial to have a damper with a larger on-state damping coefficient and a lower off-state damping coefficient. Therefore, the objective functions were to maximize the on-state damping coefficient and minimize the off-state damping coefficient. The multi objective genetic algorithm (MOGA) technique was employed to calculate the optimal particle size and weight fraction that fulfils the conflicting criteria of the objective functions. Regression analyses were performed to relate the independent and response variables using MATLAB™ software[39].

3 Results and Discussion

3.1 Damper design, manufacture and characterization

Table 1 presents the minimum and maximum limits for the design parameters, as well as the optimum dimensions for the piston.

The piston is enclosed by a gun metal cylindrical sheet of 1 mm thick. This sheet serves as a seal and prevents any leaking of MRF into the region where the piston coil is located. The cylinder's inner diameter was selected to be 30 mm in order to provide a shear gap of 0.5 mm between the internal surface of the cylinder and the external surface of the piston when they are assembled together. The cylinder has a thickness of 2 mm and its length was selected to meet the extreme stroke length of the piston, which is ± 20 mm from the mean position. The cylinder's overall length was selected as 120 mm, resulting in compressed and expanded lengths of the damper of 184 mm and 275 mm respectively. A total of 240 windings of 26 AWG copper coils were wrapped around a piston core of 14 mm diameter. The maximum current that can flow through a 26 AWG wire is 2.2 A[40]. The selection of SAE 1020 steel for the piston, piston rod, and cylinder was based on its mechanical properties, superior relative magnetic permeability and magnetic saturation. The MR damper was constructed according to the design depicted in Figure 5.

Table 1 — Bounds and optimized dimensions of the damper piston.

Parameters	Minimum limit (mm)	Maximum limit (mm)	Optimal Dimensions (mm)
Diameter of piston (D_p)	25	50	28.7
Diameter of piston rod (d_r)	8	12	10
Piston height (L_p)	30	50	30
Total piston flange height (L)	6	12	12

Figure 6 (a)-(d) shows the force as a function of displacement for the damper filled with MRF 132DG™ fluid at frequencies of 0.5 hertz, 1.0 hertz, 2.0 hertz, and 4.0 hertz, the damper coil was supplied with currents of 0A, 1A, and 2A, respectively.

An increase in frequency or current results in a corresponding increase in damping force. However, the increase in damping force with increment in applied current is more substantial compared to that with increase in frequency. The maximum force achieved during damper testing with a sinusoidal excitation of 4 Hertz for current magnitudes of 0A, 1A, and 2A are 389.6 N, 526.4 N, and 709.5 N, respectively.

3.2 Comparative analysis of experimental and computational damping force

Experimentally measured dampening force of damper with MRF 132DG™ fluid were validated with computational results.

Figures 7 (a) and 7 (b) show the geometric quarter model of the damper piston model before and after it has been meshed. A highly refined mesh was utilized in the MR fluid flow gap and piston flange area. Figures 7 (c) and 7 (d) illustrate the magnetic flux in the damper and the field strength in the MR fluid flow gap, respectively, at a current of 2 A. There is leakage of flux to MRF above and below the piston and leakage is more on the piston rod side as piston rod is made of magnetic material. It is preferred to select piston rod of non-magnetic stainless-steel material to

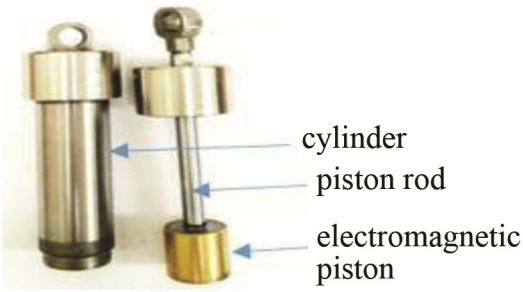

Fig. 5 — Manufactured MR damper.

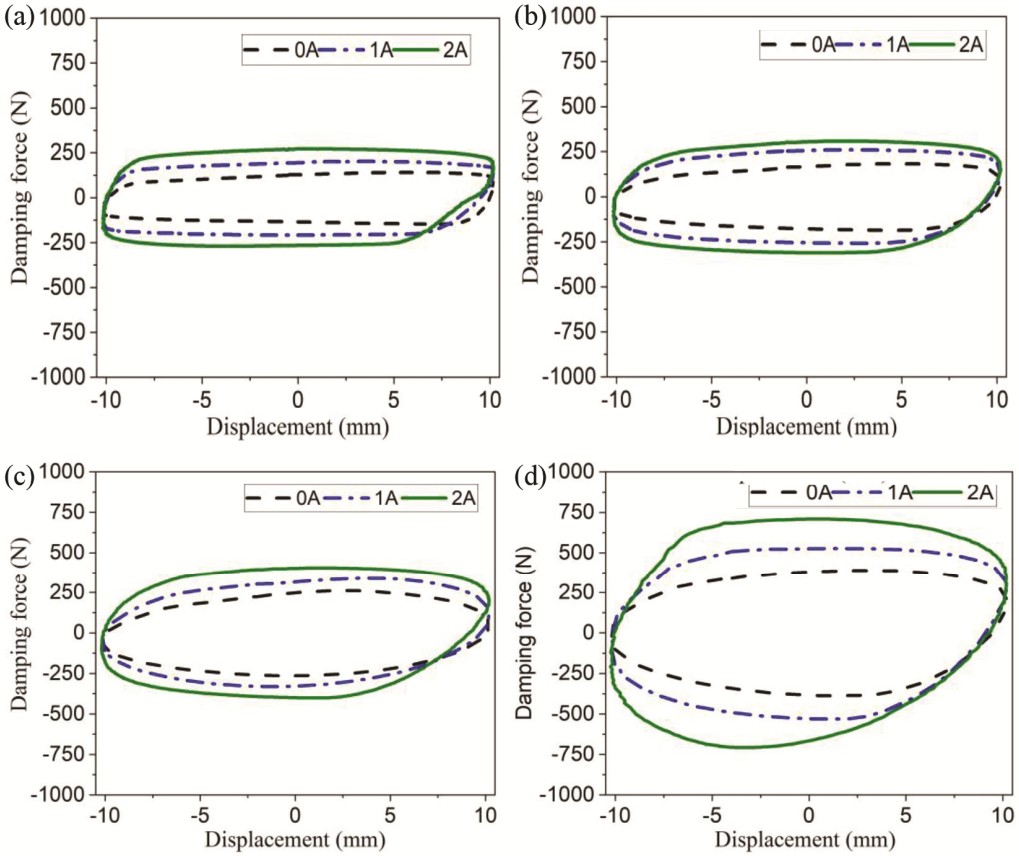

Fig. 6 — Force-displacement curves of damper with MRF 132DG^{TM} at (a) 0.5 H2, (b) 1.0 H2, (c) 2.0 H2 and (d) 4.0 H2 sinusoidal excitation frequencies.

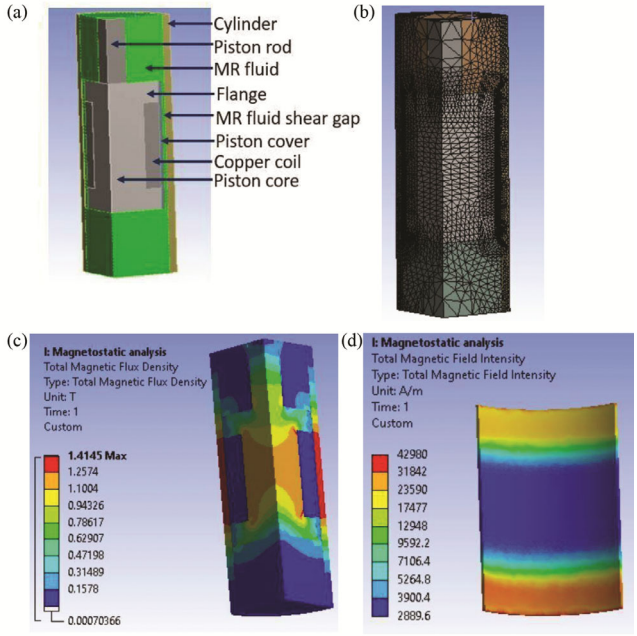

Fig. 7 — (a) MR damper's geometric model, (b) Meshing model, (c) Magnetic flux within the damper and (d) Magnetic field intensity within the MRF shear gap.

Table 2 — Damping force determined from computations and experiments.

Current (A)	Computed field induced force, F_τ(N)	Total force, Computational $(F_\tau + F_\mu)$ F (N)	Experimental force, F_E (N)
0	0	313.4	389.6
1	177.4	490.8	526.4
2	438.3	751.7	709.5

avoid leakage of magnetic field. The magnetic field varies along the height of MRF shear gap and the MRF in the vicinity of the piston flange has higher values in the top and bottom regions. The magnetic field around the piston flange is below 31.8 kA per meter. Similarly, the magnetic field intensity in the shear gap around the piston flange is determined by magnetostatic analysis at a current magnitude of 1 A.

The damping force in the off-state (F_μ) was calculated at a frequency of 4 Hertz (0.2512 m/s) and found to be 313.4 N. The total damping force (F= $F_\tau + F_\mu$) values obtained from magnetostatic analyses and analytical equations at various supplied currents were compared with the experimentally measured values listed in table 2.

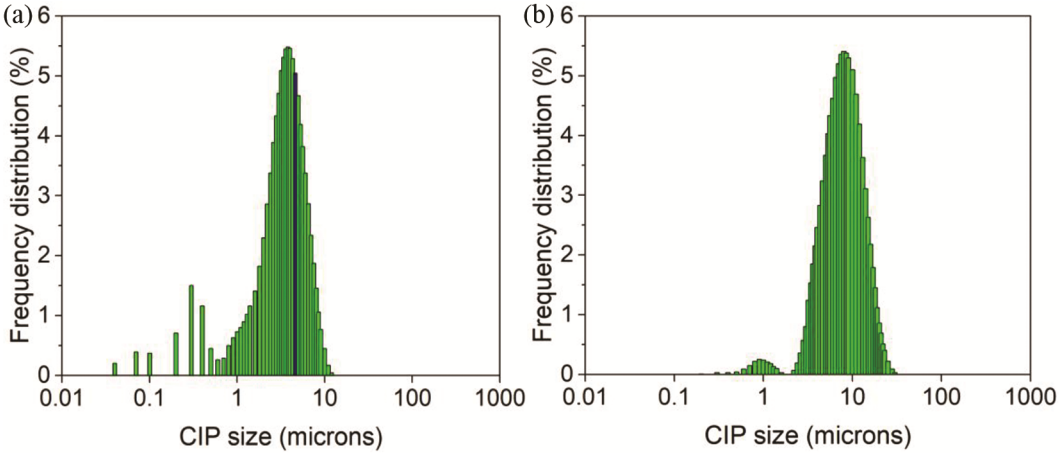

Fig. 8 — Size Distribution of (a) SCIP and (b) LCIP.

The damping force that was measured through experimentation in the absence as well as presence of current supplied to damper coil, agree well with those obtained using computational method. The discrepancy between the computed and experimentally determined damping force can be traced to the omission of friction force in the analytical equations, which occurs when no current is supplied. When a magnetic field is present, the deviation can be explained by changes in magnetic characteristics caused by flaws in the material, as well as the friction force, which is not taken into account in analytical calculations. In addition, the magnetostatic analysis does not consider the impact of temperature rise on the magnetic characteristics of the damper material and the viscosity of the magnetorheological fluid[41].

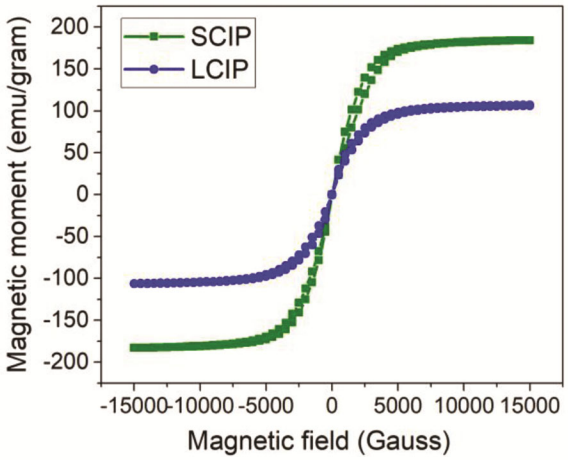

Fig. 9 — Magnetic hysteresis curves SCIP and LCIP iron powders.

3.3 MRF characterization

Figures 8 (a & b) depict the distribution of finer sized (SCIP) and coarser sized CIP (LCIP). Mean diameters of SCIP and LCIP are 2.9 and 8.27 microns respectively.

The magnetization curves of iron powders are shown in Fig. 9. The magnetic saturation of SCIP and LCIP are 184.2 emu/g and 106.9 emu/g while the coercivity of SCIP and LCIP are 0.59 and 3.85 respectively. Hence, finer sized CIP (SCIP) possess superior magnetic properties since it has higher magnetic saturation than that of coarser size CIP (LCIP) while SCIP has lower coercivity than that of LCIP, which is desirable for reversibility of MR effect. Higher magnetic saturation of iron powder yields higher shear stress MRF[42].

The flow curves for MRF with 60%, 70%, and 80% weight percentages of fine and coarse CIP are displayed at zero magnetic field in Fig. 10 (a). It is evident that an MRF with a larger weight percentage of CIP produces a higher shear stress due to its increased viscosity. Moreover, MRF made of fine CIP have higher shear stress than MRF made of coarse CIP for all weight fractions because MRF with fine-sized CIP would include more particles overall. MRF 132DG^{TM} fluid has lowest off-state shear stress compared to prepared MRF, lesser than MRF composed of 60% weight fraction of CIP. This indicates that MRF 132DG^{TM} fluid has lowest viscosity since shear stress and viscosity are directly proportional to each other. MRF 132DG^{TM} has 80.98% mass fraction of magnetic phase as per product data sheet. The viscosity of MRF depends on the carrier oil viscosity and the weight fraction of iron powder in it. Hence, carrier oil of very low viscosity has been utilized in MRF 132DG^{TM} fluid.

Figures 10 (b)-10 (d) display the flow curves for MRF containing different weight percentages of particles (60%, 70%, and 80%). These particles

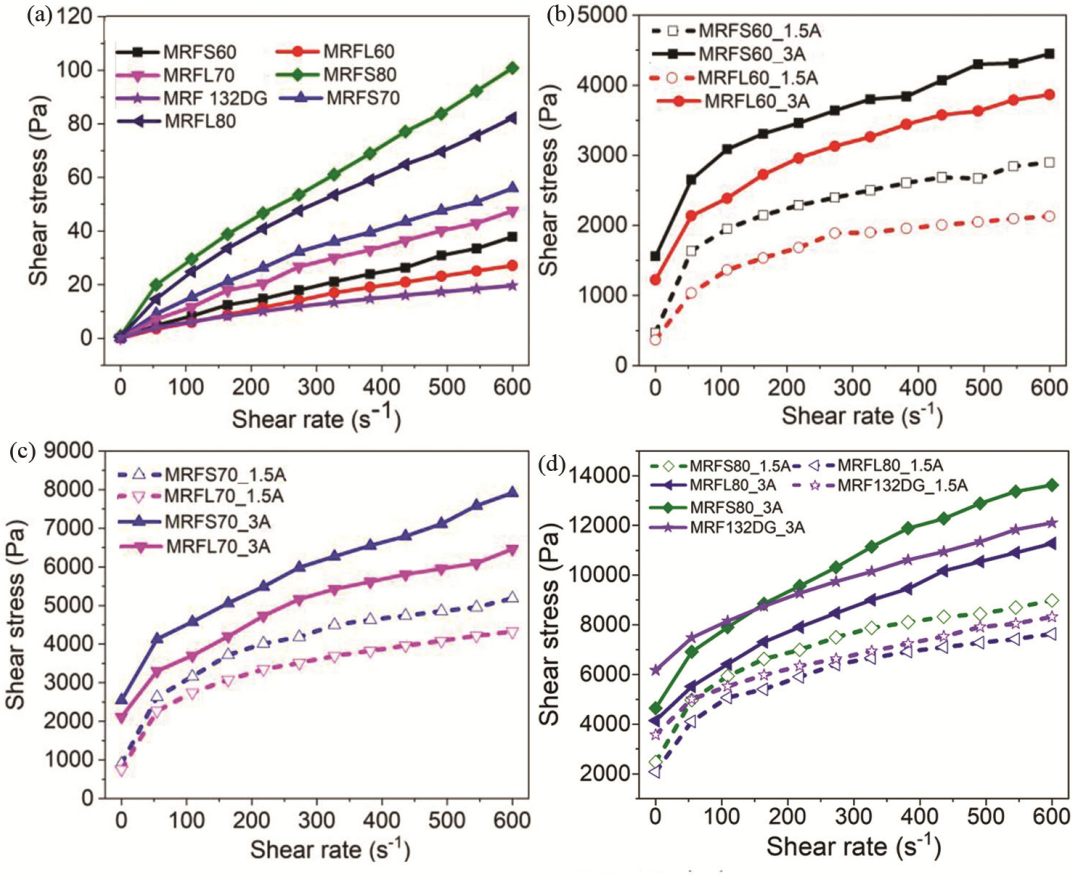

Fig. 10 — Flow curves of MRFs in the (a) absence of current; and presence of current for (b) 60% CIP weight fraction, (c) 70% CIP weight fraction and (d) 80% CIP weight fraction, MRF 132DG fluid.

consist of both fine and coarse sized Carbonyl Iron Powder (CIP). The flow curves were obtained at currents of 1.5 A and 3 A. It is clear that, regardless of the particle weight fractions, MRFs consisting of SCIP exhibit higher shear stress in comparison to ones composed of LCIP. This is due to the observation that SCIP has a larger saturation magnetization than LCIP based on magnetic property testing results. Figure 10 (d) displays the flow curves of MRF 132DG^{TM} for comparison with the flow curves of an In-house MRF consisting of 80% weight fractions of CIP of SCIP and LCIP. The reason for this is because MRF 132DG^{TM} consists of 80.98% by weight fraction of magnetic particles as per product data sheet. It can be observed that except at very low shear rates, the shear stress of MRF 132DG^{TM} fluid are less than those obtained for MRF80S and more than those of MRF80L. This could be attributed to superior magnetic properties of SCIP which has saturation magnetization of 184.2 emu/g and higher viscosity of the MRF containing SCIP (MRFS80). However, MRFL80 has lesser shear stress than MRF 132DG^{TM} as it is composed of LCIP which has low saturation magnetization of 106.9 emu/g.

Sedimentation ratio for different MRF were plotted at intervals of twelve hours as shown in Figure 11(a). MRF composed of coarse sized iron particles settle faster than those consisting of fine sized iron particles for all weight fractions. This indicates that SCIP have better sedimentation stability and have been reported by researchers in literature[1,43]. Also, MRF with higher particle weight fraction have higher sedimentation ratio as settling rate of particles is lesser[44-45]. MRF composed of 80% weight fraction of SCIP has sedimentation ratio of 72 hrs which is the maximum among prepared MRF as it contains and highest weight fraction of SCIP. Likewise, MRF with 60% weight fraction of LCIP has minimum stability of 27 hours as it is composed of coarse sized CIP of lowest weight fraction. Figure 11(b) shows MRF which have completely settled in the graduated cylindrical measuring tubes.

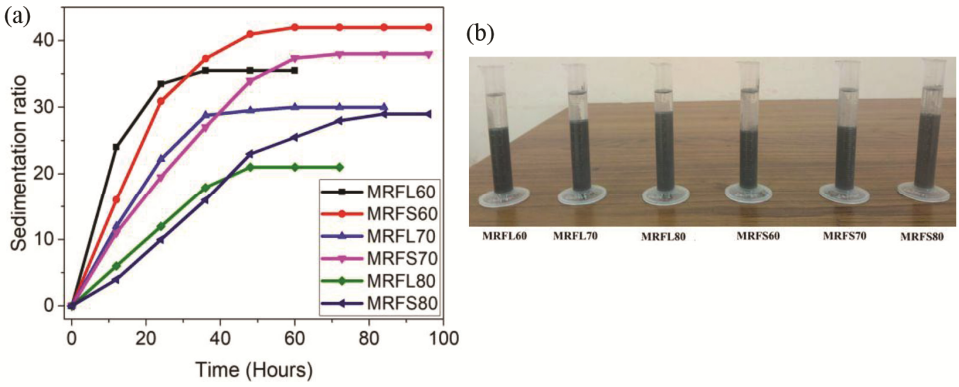

Fig. 11 — (a) Sedimentation ratio as a function of time for MRFs and (b) MRFs after complete particle settling.

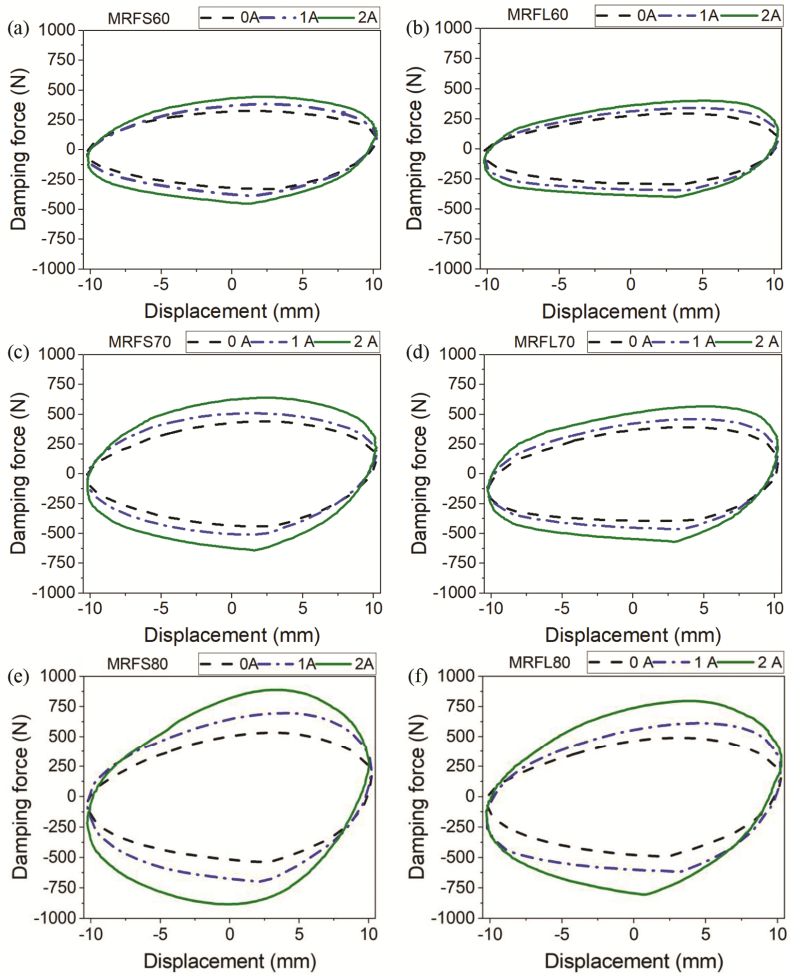

Fig. 12 — (a, c, e) Force characteristic curves with variation in current and weight fraction and (b, d, f) Fine sized CIP and Coarse sized CIP.

3.4 Damper characterization

Figures 12(a), 12(c), and 12(e) display the force displacement plots of a MR damper using different weight fractions (60%, 70%, and 80%) of SCIP based MRF. Similarly, Figures 12(b), 12(d), and 12(f) show the force displacement plots of a damper using different weight fractions (60%, 70%, and 80%) of LCIP based MRF. An increase in the weight proportion of iron particles in the magnetorheological fluid results in a corresponding rise in the damping force. This is due to the larger quantity of iron particles, which leads to a greater magnetorheological

effect. The use of MRF with smaller particle size (SCIP) resulted in increased damper force, primarily due to its greater magnetic saturation. As the current given to the piston coil increases, the damping force also increases significantly compared to the off-state condition, where no current is supplied. Additionally, damper force increases for all weight fractions and particle sizes as the excitation frequency increases. Damper filled with MRF 132DG^{TM} fluid (figure 6 (d)) yielded damping force lesser than those of MRFL80 (figure 12 (f)) and MRFS80 (figure 12 (e)) while its higher than MR fluid consisting of 60% and 70% weight fractions of LCIP and SCIP. At 4 Hertz excitation frequency and supply current of 2 A, MRF 132DG^{TM} fluid yielded a damping force of 709.5 N while MRFL80 and MRFS80 yielded 796.5 N and 889.1 N respectively. This can be due to a smaller concentration of magnetic field strength in the MRF shear gap, which leads to a reduced contribution of the on-state damping force. When it comes to fluids made in-house, the viscous damping force makes a considerable contribution to the overall damper force due to their higher viscosities. Similar behaviour was observed between the inhouse and commercial MRF at other excitation frequencies i.e. 0.5 Hertz, 1 Hertz and 2 Hertz. The force-displacement curves of the Magnetorheological Fluid (MRF) were evaluated at various frequencies.

Figure 13 (a) illustrates the impact of the size and weight percentage of CIP on the off-state damping coefficient.

The variation shows that the off-state damping coefficient significantly increases as the weight fraction of CIP increases, but there is a slight drop in the off-state damping coefficient with an increase in particle size. This is due to the fact that when the particle size increases, the viscosity of the magnetorheological fluid (MRF) lowers, resulting in a drop in shear stress and force. Figure 13 (b) illustrates the impact of the size and weight percentage of CIP on the damping coefficient in the on-state. The damping coefficient in the on-state significantly increases as the weight percentage of particles increases. Magnetorheological fluids (MRF) made of SCIP have a larger damping coefficient compared to MRF composed of LCIP. This is attributed to the superior shear stress of MRF composed of SCIP, as seen from their flow curves. Based on the slope of surface plots, it is evident that the weight fraction of iron particles in MRF has a substantial impact on the damping coefficient, in comparison to the particle size.

3.5 Selection of optimum weight fraction and particle size

The dependent variables in this study are the on-state damping coefficient and off-state damping coefficient. On the other hand, the independent factors include the particle size (P_S) and particle weight fraction (W_F). The equation (9) is the regression model for the off-state damping coefficient, using R-square and adjusted R-square values of 1 and 0.9999, respectively.

$$\text{Damping coefficient (Off-state)} = 598.9 + 16.75*P_S - 17.92*W_F - 0.353*P_S*W_F + 0.2312*W_F*W_F \quad \ldots (9)$$

The equation (10) is the regression model for the on-state damping coefficient of a damper, with R-Square and adjusted R-square values of 0.9999 and 0.9994, respectively.

$$\text{Damping coefficient (On-state)} = 1143 - 26.39*P_S - 32.57*W_F + 0.1662*P_S*W_F + 0.3837*W_F*W_F \ldots (10)$$

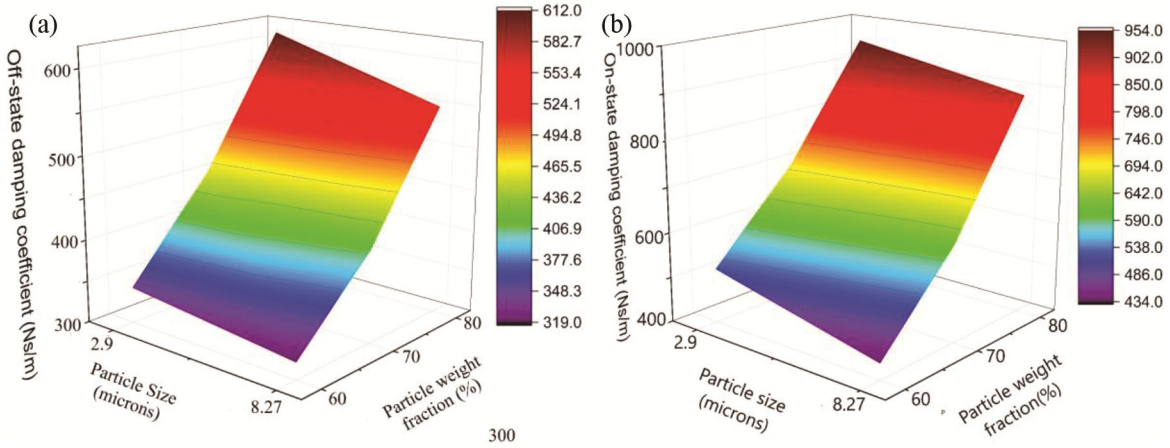

Fig. 13 — Effect of independent factors on damping coefficients (a) Off state and (b) On-state.

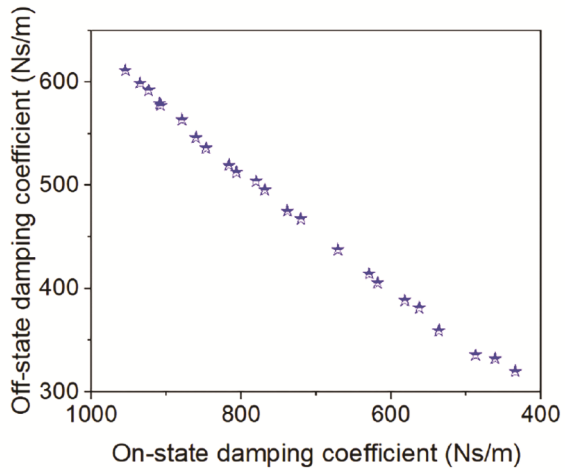

Fig. 14 — Pareto front graph.

The MOGA optimization conducted using MATLAB^{TM} software yields a collection of solutions that meet the criteria of the objective functions, referred to as the pareto front graph, as depicted in Figure 14. A magnetic rheological fluid (MRF) with a particle size of about 3 µm (3.03 µm) and a particle weight fraction of 73.56% was selected. This MRF exhibits an on-state damping coefficient of 780.5 Ns/m and an off-state damping coefficient of 503.8 Ns/m. A smaller particle size was selected due to its superior sedimentation stability and lesser particle wear. Higher weight fraction of CIP yields higher on-state and off-state damping coefficients and vice-versa. Hence, slightly lower weight fraction of CIP was chosen from pareto front to ensure fairly higher on-state damping coefficient and lower off-state damping coefficient.

4 Conclusion

In this study, by means of optimization technique, a shear mode MR damper was specifically engineered to achieve a desired level of damping force and to operate within a specific dynamics range. The damper was manufactured using the optimal dimensions and filled with MRF 132DG^{TM} to assess its damping properties. The damper's performance was then confirmed by comparing it to computational results. In addition, MRF were prepared using iron particles with weight fractions of 60%, 70%, and 80%, consisting of both finer and coarser particle sizes. The flow curves of the In-house prepared MRF and MRF 132DG^{TM} were measured using rheometer. Sedimentation stability of the In-house prepared MRFs were determined. The MR damper was filled with in-house prepared magnetorheological fluid and the damper characteristics were measured under sinusoidal excitation with a piston stroke of ±10 mm at various frequencies. The measurements were conducted without current and with DC current inputs of 1A and 2A. The energy dissipated was calculated using the area enclosed by the force-displacement curves which was subsequently used to evaluate the equivalent damping coefficient. To end with, the optimal weight fraction and particle size of iron powder were determined using MOGA optimization, on the basis of maximizing the on-state damping coefficient and minimizing the off-state damping coefficient. From this study, following conclusions were drawn.

- The MR damper, filled with MRF 132DG^{TM}, which was developed and manufactured provided a maximum damping force of 709.5 N when subjected to a sinusoidal excitation with a frequency of 4 Hertz and a current of 2A. The damping force, calculated using magnetostatic investigations and mathematical calculations, is nearly 751.7 N. A considerable degree of agreement in the outcomes between the two was noted.
- The damping force loaded with MRF 132DG^{TM} was found to be lower than the damping forces obtained for in-house made MRFs containing 80% weight fraction of iron powder. This can be due to a reduced concentration of magnetic field in the gap of the MR fluid, which leads to a decrease in the contribution of field induced damping force to overall force. When using the prepared fluid, the viscous damping force makes a considerable contribution to the overall damping force.
- The Rheometer readings of flow curves showed that the Magnetorheological Fluid (MRF) containing fine-sized Carbonyl Iron Powder (CIP) exhibited increased shear stress as the shear rate varied. This can be attributed to the higher magnetic saturation of the fine-sized CIP.
- MRF made with fine-sized carbonyl iron particles (SCIP) have a slower settling rate compared to those made with coarse-sized (LCIP). They take a longer time to settle, which indicates a higher level of sedimentation stability in MRF made with fine-sized CIP. Increasing the weight percentage of carbonyl iron particles (CIP) in the magnetorheological fluid (MRF) led to a corresponding increase in the damping force.

Furthermore, augmenting the electric current supplied to the MR damper piston coil resulted in an increase in the damping force. The damping force likewise escalates with an increase in the frequency of excitation.

- The MRF consisting of fine sized CIP exhibited greater damping force and an equivalent damping coefficient compared to the MRF consisting of coarse CIP. This is attributed to the fine-sized CIP's higher magnetic saturation and shear stress in comparison to its coarse counterpart.
- The weight fraction of CIP in MRF has a substantial impact on the equivalent damping coefficient, in comparison to the particle size.
- An optimum magnetorheological fluid (MRF) for a damper was proposed, consisting of particles with an average size of around 3 μm and a particle weight fraction of 73.56%. This MRF exhibits an on-state damping coefficient of 780.5 Ns/m and an off-state damping coefficient of 503.8 Ns/m.

The proposed approach in this study could be used for optimum choice of composition of MR fluid for MR damper from various blends of magnetic phase, carrier oil, additives and their proportions.

Acknowledgment

The authors are grateful to the support provided by Central Research Facility, National Institute of Technology Karnataka, Surathkal for providing rheometer test facility.

Conflict of Interest

The authors have no conflicts of interest to declare that are relevant to the content of this article.

Funding

This research was supported by funding from the Ministry of Human Resource Development and the Ministry of Road Transport and Highways, Government of India, under the IMPRINT Project [Grant No. IMPRINT/2016/7330] titled ‘‘Development of Cost Effective Magnetorheological (MR) Fluid Damper in Two wheelers and Four Wheelers Automobile to Improve Ride Comfort and Stability’’.

References

1 Gołdasz J & Sapinski B, Insight into magnetorheological shock absorbers (Springer International Publishing, Switzerland),1st Edn, ISBN: 978-3-319-35747-8, 2015, p. 14.
2 Ahmad S, *Indian J Eng and Mater Sci,* 12 (2005) 299.
3 Rabinow J, *Trans. Am Inst Electr Eng,* 67 (1948) 1308.
4 Choi S B & Han Y M, Magnetorheological Fluid Technology: Applications in Vehicle Systems (Taylor & Francis, Boca Raton), 1st Edn, ISBN: 9781138076365, 2012, p. 142.
5 Klingenberg D J, *JAIChE,* 47 (2001) 246.
6 Ahamed R, Choi S B & Ferdaus M M, *J Intell Mater Syst Struct,* 29 (2018) 2051.
7 Wang J & Meng G, *Proc Inst Mech Eng Pt L J Mater Des Appl,* 215 (2001) 165.
8 Allien J, Kumar H & Desai V, *Proc Inst Mech Eng Pt L J Mater Des Appl,* 234 (2020) 574.
9 Shubham V, Neelesh K & Amod K, *Indian J Eng and Mater Sci,* 72 (2013) 213.
10 Girinath B, Mathew A, Babu J, Thanikachalam J, Bose S S, *Indian J Eng and Mater Sci,* 77 (2018) 35.
11 Nikitin L V, *Indian J Eng and Mater Sci*, 11 (2004) 295.
12 Spaggiari A, Castagnetti D, Golinelli N, Dragoni E & Scirè Mammano G, *Proc Inst Mech Eng Part L J Mater Des Appl,* 233 (2019) 734.
13 Nguyen Q H, Choi S B & Wereley N M, *Smart Mater Struct,* 17 (2008) 025024.
14 Naserimojarad M M, Moallem M & Arzanpour S, *J Intell Mater Syst Struct,* 29 (2018) 3648.
15 Parlak Z, Engin T & Callı T, *Mechatron,* 22 (2012) 890.
16 Gurubasavaraju T M, Kumar H & Arun M, *J Braz Soc Mech Sci Eng,* 39 (2017) 2225.
17 Nguyen Q H, Choi S B, Lee Y S & Han M S, *Smart Mater Struct,* 18 (2009) 095032.
18 Parlak Z, Engin T & Sahin I, *J Mech Des,* 135 (2013) 081008.
19 Xu Z D, Sha L F, Zhang X C & Ye H H, *Struct Control Health Monit,* 20 (2013) 956.
20 Desai R M, Jamadar M E H, Kumar H, Joladarashi S & Raja Sekaran S C, *J Braz Soc Mech Sci Eng,* 4 (2019) 332.
21 Madhavrao Desai R, Acharya S, Jamadar M E H, Joladarashi S & Raja Sekaran S C,*Proc Inst Mech Eng Pt L J Mater Des Appl,* 234 (2020) 1001.
22 Puneet N P, Devikiran P, Kumar H & Gangadharan, K V, *JVib Eng Technol*, 10 (2022) 967.
23 Gurubasavaraju T M, Kumar H & Arun M, *J Braz Soc Mech Sci Eng,* 39 (2017) 3683.
24 Mangal S K & Sharma V, *J Braz Soc Mech Sci Eng,* 39 (2017) 4191.
25 Acharya S, Saini T R S, Sundaram V & Kumar H, *J Intell Mater Syst Struct,*32 (2020)1831.
26 Acharya S, Vipin J A, Puneet N P & Kumar H, *Int J Smart Nano Mater,* 12 (2021) 88.
27 Acharya S, Saini T R S & Kumar H, *J Braz Soc Mech Sci Eng,* 41 (2019) 392.
28 Choi Y T & Wereley N M, *J Aircr,* 40 (2003) 432.
29 Yang G, Spencer B F, Carlson J D & Sain, M K, *Eng Struct,* 24 (2002) 309.
30 https://lordfulfillment.com/pdf/44/DS7015_MRF-132DGMRFluid.pdf (12 June 2020)
31 https://magweb.us/smag/(05 June 2020)
32 Gao F, Liu Y N & Liao W H, *Smart Mater Struct,* 26 (2017) 035034.
33 Yoo J H & Wereley N M, *J Intell Mater Syst Struct,* 13 (2002) 679.

34 Hu G, Xie Z & Li W, *Proc 11th World congr Struct and Multidiscip Optim,* Sydney, Australia, June 07-12, (2015), 2.
35 Zuzhi T, Fei C, Xiangfan W & Jian W, *Mater Manuf Process,* 31 (2016) 2030.
36 López-López M T, Zugaldia A, González-Caballero F, & Duran J D G, *J Rheol,* 50 (2006) 543.
37 Ashtiani M, Hashemabadi S H, *J Intell Mater Syst Struct,* 26 (2018) 1887.
38 Rao SS & Yap FF, Mechanical Vibrations (Prentice Hall, Upper Saddle River), 5th Edn, ISBN: 978-0-13-212819-3, 2012, p. 46.
39 Puneet N P, Hegale A, Kumar H & Gangadharan K V, in Recent Advances in Computational Mechanics and Simulation, Lecture Notes in Mechanical Engineering, edited by Saha S K, Mukharjee M (Springer Publishers, Singapore), 2021, 623.
40 https://powerstream.com/Wire_Size.htm (05 June 2020)
41 Karakoc K, Park E J & Suleman A, *Mechatron,* 18 (2008) 434.
42 Genc S & Phulé PP, *Smart Mater Struct,* 11 (2002) 140.
43 Zhang Q, Liu X, Ren Y, Wang L, Hu Y, *Adv Mater Sci Eng,* 2016 (2016) 1.
44 Ngatu G T & Wereley N M, *IEEE T Magn,* 43 (2007) 2474.
45 Liu X, Lu H, Chen Q, Wang D & Zhen X, *Mater Manuf Process,* 28 (2013) 631.